Low Temperature Physics/Fizika Nizkikh Temperatur, 2011, v. 37, Nos. 9/10, p. 943–949

Magnetoresistance oscillations up to 32 K in the organic metal β″-$(ET)_4(H_3O)[Fe(C_2O_4)_3]\cdot C_6H_4Cl_2$

Vladimir N. Laukhin[1,2], Alain Audouard[3], David Vignolles[3], Enric Canadell[2], Tatyana G. Prokhorova[4], and Eduard B. Yagubskii[4]

[1]*Institució Catalana de Recerca i Estudis Avançats, 08010 Barcelona, Spain*
[2]*Institut de Ciència de Materials de Barcelona, Consejo Superior de Investigationes Científicas, Campus Universitat Autònoma de Barcelona, Bellaterra 08193, Spain*
[3]*Laboratoire National des Champs Magnétiques Intenses (UPR 3228 CNRS, INSA, UJF, UPS) 143 avenue de Rangueil, F-31400 Toulouse, France*
[4]*Institute of Problems of Chemical Physics, Russian Academy of Sciences, 142432 Chernogolovka, MD, Russia*
E-mail: vladimir@icmab.es

Received February 2, 2011

Magnetic torque and magnetoresistance of the quasi-two-dimensional charge transfer salt β″-$(ET)_4(H_3O)[Fe(C_2O_4)_3]\cdot C_6H_4Cl_2$ have been investigated in pulsed magnetic fields of up to 55 T. At variance with de Haas–van Alphen oscillations, Shubnikov–de Haas oscillations are observed up to temperatures as high as 32 K at ambient pressure despite a significant thermal damping in the low-temperature range. This feature, observed under applied pressure as well, is interpreted on the basis of the coexistence of a closed orbit and a quantum interference path with the same cross section.

PACS: **71.18.+y** Fermi surface: calculations and measurements; effective mass, *g* factor;
71.20.Rv Polymers and organic compounds;
72.15.Gd Galvanomagnetic and other magnetotransport effects.

Keywords: quantum oscillations, Fermi surface, organic metals, high magnetic fields.

1. Introduction

Charge transfer salts β″-$(ET)_4(A)[M(C_2O_4)_3]\cdot Solv$ (where ET stands for bis-ethylenedithio-tetrathiafulvalene, A is a monovalent cation, M is a trivalent cation and Solv is a solvent) make up a family of organic compounds which have raised great interest for many years [1]. These salts which share the same generic formula and β″ packing of the ET molecules can be either orthorhombic, in which case they are insulating, or monoclinic quasi-two-dimensional (q-2D) metals. Among these latter salts, denoted as (A, M, Solv) hereafter, many different ground-states, including normal metal, charge density wave, superconductivity, and temperature-dependent behaviors can be observed.

According to band structure calculations [2], the Fermi surface (FS) of organic metals with such packing, originates from a hole orbit (labelled ⊙ in the following) with an area equal to that of the first Brillouin zone (FBZ). In the case of (NH_4, Fe, C_3H_7NO), a small gap opening is predicted at the point *Y* of the FBZ yielding compensated orbits with much smaller area (8.8% of the FBZ, according to [3]), as displayed in Fig. 1(b). However, the Fermi level is very close to the band extrema at *Y* which can make the actual FS topology very sensitive to subtle structural details. Namely, if the gap is larger than in the case of Fig. 1(b), the electron-type orbits transform into quasi-one dimensional sheets as displayed in Fig. 1(a). Oppositely, in the case where the gap is closed, ⊙ orbits intersect along two directions. An additional orbit is then observed and the FS topology is similar to that of Fig. 1(c) [4] with two hole and one electron compensated orbits.

Of course, phase transition such as density wave condensation can drastically change the FS topology at low temperature. As a matter of fact, depending on the studied compound and external parameters such as a moderate applied pressure, Shubnikov–de Haas (SdH) oscillations spectra have revealed from one to six Fourier components in this family [5–10]. Their frequency are in the range 40 to 350 T that corresponds to orbits with area ranging from 2 to 18% of the FBZ area. In most cases, these orbits are compensated, in agreement with band structure calculations. For example, SdH data of (NH_4, Fe, C_3H_7NO) collected up to applied pressures of 1 GPa [5,10], can be interpreted on the basis of three compensated orbits

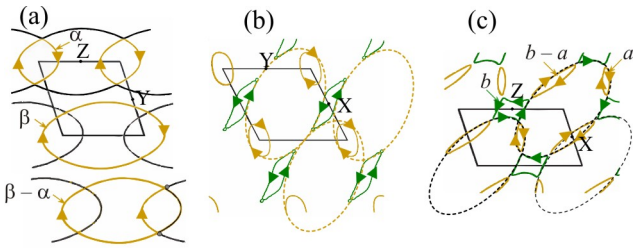

Fig. 1. Fermi surface of $(BEDO)_5Ni(CN)_4{\cdot}4CH_3CN$ [4] (a), β″-$(ET)_4(NH_4)[Fe(C_2O_4)_3]{\cdot}C_3H_7NO$ [3] (b) and $(BEDO)_4Ni(CN)_4{\cdot}3C_2H_4(OH)_2$ [4] (c). Ellipses in dashed lines stand for intersecting hole orbits with area equal to that of the First Brillouin zone (⊙ orbits). They lead to three compensated electron (*b*) and hole (*a* and *b*–*a*) orbits in (c). β orbits in (a) correspond to ⊙ orbits. The arrows indicate the quasiparticles direction.

corresponding to the textbook case reported in Fig. 1(c), where a and $b-a$ are hole orbits while b is an electron orbit. Oscillatory spectra of (NH_4, Fe, C_3H_7NO), in which the only difference with the former salt is that Fe^{3+} ions are changed by Cr^{3+}, are also in agreement with a FS such as in Fig. 1(c) for applied pressures above 0.8 GPa. However, at variance with this feature, it exhibits six Fourier components at ambient pressure [9].

The present paper reports on both magnetoresistance and torque experiments performed up to 55 T on (H_3O, Fe, $C_6H_4Cl_2$). Even though the oscillatory spectra can be accounted for by the three compensated orbits a, $b-a$ and b, the main result is the persistence of the b oscillations in SdH data at temperatures as high as 32 and 25 K at ambient pressure and 0.5 GPa, respectively. This feature, which is not observed in de Haas–van Alphen (dHvA) spectra is discussed on the basis of the presence of both a quantum interferometer and a closed orbit with the same area. Although the observed frequencies are in agreement with the predictions of band structure calculations, this behavior points to a FS reconstruction at low temperature.

2. Experimental

The studied crystals were synthesized by electrocrystallization technique as reported in Ref. 3. Magnetoresistance and magnetic torque were measured in pulsed magnetic fields of up to 55 T with a pulse decay duration of 0.32 s.

For magnetoresistance measurements, the studied crystals were elongated hexagonal platelets with approximate dimensions 0.4×0.2×0.1 mm, the largest faces being parallel to the conducting *ab* plane. Electrical contacts were made using annealed platinum wires of 20 μm in diameter glued with graphite paste. Alternating current (100 μA, 50 kHz) was injected parallel to the c^* direction (interlayer configuration). The explored temperature range was from 1.4 to 32 K. For experiments at ambient pressure, a one-axis rotating sample holder allowed to change the angle (θ) between the direction of the magnetic field and the c^* crystal axis. Interlayer magnetoresistance was also measured under hydrostatic pressure of 0.5 GPa in a calibrated anvil cell [11] with the magnetic field perpendicular to the conducting plane.

Magnetic torque measurements were performed with a commercial piezoresistive microcantilever [12] in the temperature range from 1.9 to 15 K. The crystal size was approximately 0.3×0.1×0.07 mm. Variations of the cantilever piezoresistance was measured with a Wheatstone bridge with an *ac* excitation at a frequency of 63 kHz. A lock-in amplifier with a time constant in the range 30–100 μs was used to detect the measured signal for magnetoresistance and torque measurements. Discrete Fourier analysis of the oscillatory part of the data, obtained after suppression of a nonoscillating background were performed using Blackman-type windows.

3. Results and discussion

Several Fourier components which are linear combinations of the two frequencies F_a and F_b (in particular, $F_{b-a} = F_b - F_a$) can be distinguished in the SdH data of Fig. 2. As reported in Fig. 3, they follow the law $F(\theta) = F(\theta = 0)/\cos(\theta)$ expected for a two-dimensional FS. At ambient pressure and for $\theta = 0°$, $F_a = (74 \pm 5)$ T and $F_b = (348 \pm 3)$ T that correspond to orbits area $A_a = (1.9 \pm 0.1)\%$ and $A_b = (8.8 \pm 0.1)\%$ of the First Brillouin zone (FBZ) area, consistently with dHvA data recorded at $\theta = 29°$. At 0.5 GPa, $F_a = (82 \pm 2)$ T ($A_a = (2.1 \pm 0.1)\%$) and $F_b = (383 \pm 2)$ T ($A_b = (9.6 \pm 0.1)\%$). Taking into account the small value of the orbits area with respect to that of the FBZ, these data are not consistent with a FS such as in Fig. 1(a) but more in line with a topology analogous to Fig. 1(c). Indeed, even though analogous linear combination of frequencies ($F_\beta = F_\alpha + F_{\beta-\alpha}$) is widely observed for FS such as in Fig. 1(a), F_β which corresponds to the ⊙ orbit in this case, amounts to few thousands of teslas which is one order of magnitude larger than F_b. Oppositely, the FS of Fig. 1(c) is composed of three compensated closed orbits originating from intersecting ⊙ orbits at the *X* and *Y* points of the FBZ without gap opening at the *Y* point, yielding orbits area of the order of few percent of the FBZ in agreement with data in Figs. 2 and 3.

It can be noticed that frequencies at 0.5 GPa are by about 10 percent lower than at ambient pressure which corresponds to a pressure sensitivity $d\ln F/dP \sim -0.2\ \mathrm{GPa}^{-1}$, close to the values reported for closed orbits in other ET salts [13]. However, the most remarkable feature of the data reported in Fig. 2 is the persistence of magnetoresistance oscillations at 32 and 25 K at ambient pressure and 0.5 GPa, respectively. More insight on this feature can be derived from the field- and temperature-dependence of the oscillations amplitude. Within the Lifshits–Kosevich formalism, oscillatory parts of magnetore-

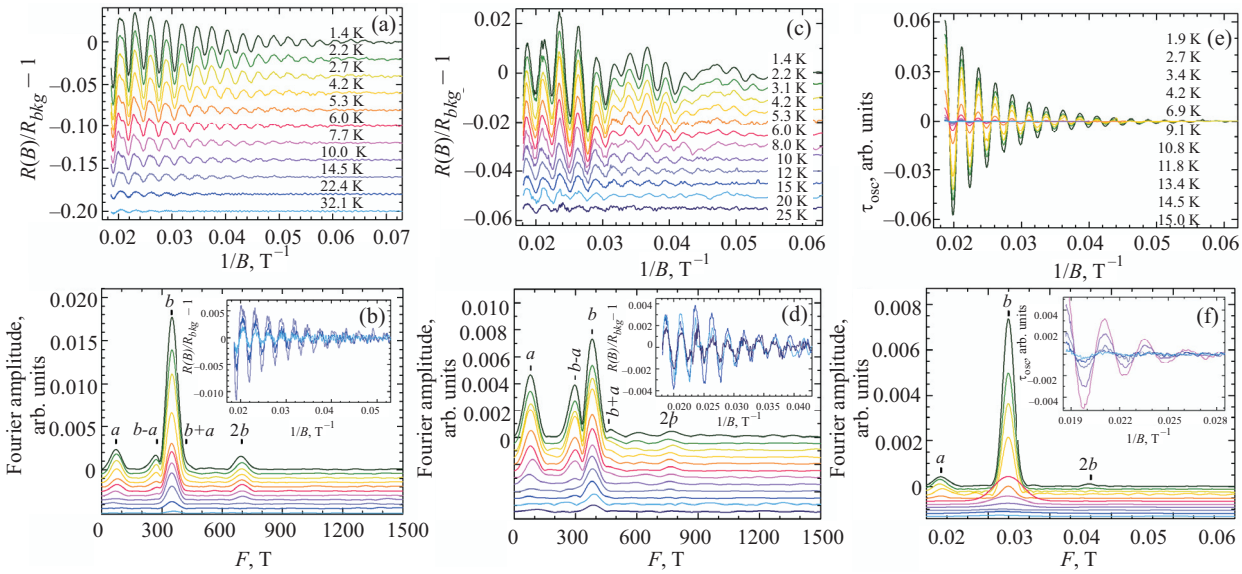

Fig. 2. Oscillatory part of the magnetoresistance data at ambient pressure (a) and 0.5 GPa (c) for θ = 0°. R_{bkg} is the nonoscillating background part of the magnetoresistance. (e) Oscillatory part of the magnetic torque for θ = 29° at various temperatures. (b), (d) and (f) Fourier spectra of data in (a), (c) and (e), respectively. Insets display oscillatory parts of the data in the high-temperature range. Curves in main panels of (a), (b), (c), (d) and (f) are shifted down from each other by a constant amount.

sistance (SdH effect) and magnetic torque (dHvA effect) can be written

$$\frac{R(B)}{R_{\text{background}}} = 1 + \sum_j A_j \cos[2\pi(\frac{F_j}{B} - \gamma_j)] \qquad (1)$$

and

$$\tau_{\text{osc}} = B \tan\theta \sum_j A_j \sin[2\pi(\frac{F_j}{B} - \gamma_j)], \qquad (2)$$

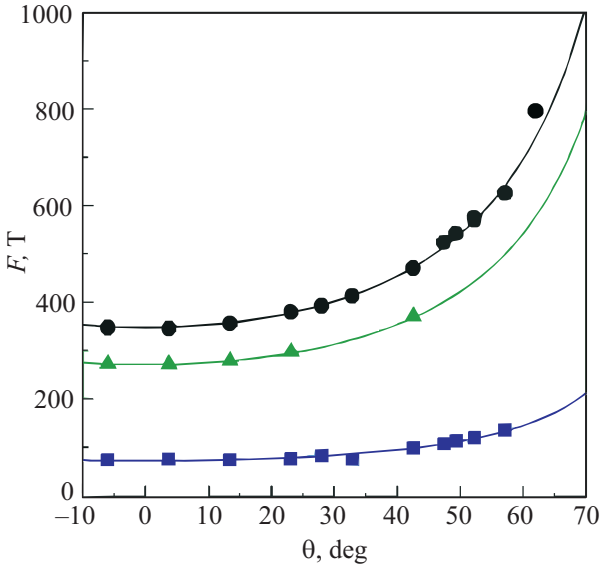

Fig. 3. Angle (θ) dependence of the frequencies F_a (solid squares), F_{b-a} (solid triangles) and F_b (solid circles). Solid lines are the best fits to $F(\theta) = F(\theta = 0)/\cos\theta$ for which F_a (θ = = 0) = 74 T and F_b (θ = 0) = 348 T.

respectively, where θ is the angle between the magnetic field direction and the normal to the conducting plane. The amplitude of the Fourier component with frequency F_j is given by $A_j = a_j R_{Tj} R_{Dj} R_{MBj} R_{Sj}$ where a_j is a constant. For a two-dimensional FS, the thermal, Dingle, magnetic breakdown (MB) and spin damping factors are, respectively, given by [14,15]

$$R_{Tj} = \frac{\alpha T m_j^*}{B\cos\theta \sinh[\alpha T m_j^* / B\cos\theta]}, \qquad (3)$$

$$R_{Dj} = \exp[-\alpha T_D m_j^* / B\cos\theta], \qquad (4)$$

$$R_{MBj} = \exp(-\frac{t_j B_0}{2B})[1 - \exp(-\frac{B_0}{B})]^{b_j/2}, \qquad (5)$$

$$R_{Sj} = \cos(\pi\mu_j / \cos\theta), \qquad (6)$$

where $\alpha = 2\pi^2 m_e k_B / e\hbar$ (≃14.69 T/K), m_j^* is the effective mass normalized to the free electron mass m_e, T_D is the Dingle temperature ($T_D = \hbar\tau^{-1} / 2\pi k_B$, where τ^{-1} is the scattering rate) and B_0 is the MB field. Integers t_j and b_j are the number of tunnelling and Bragg reflections involved in the MB orbit, respectively.

As usual, effective masses can be deduced from the temperature dependence of the oscillations amplitude through Eq. (3) (see Fig. 4). At ambient pressure and θ = 0, magnetoresistance data yield $m_a^* = 0.84 \pm 0.06$ which is in good agreement with data from de Haas–van Alphen oscillations ($m_a^* = 0.83 \pm 0.20$). A lower value ($m_a^* = 0.72 \pm 0.08$) is obtained at 0.5 GPa. An effective mass decrease is also observed for $b-a$, namely, $m_{b-a}^* = 1.00 \pm 0.05$ and 0.82 ± 0.08 at ambient pressure and

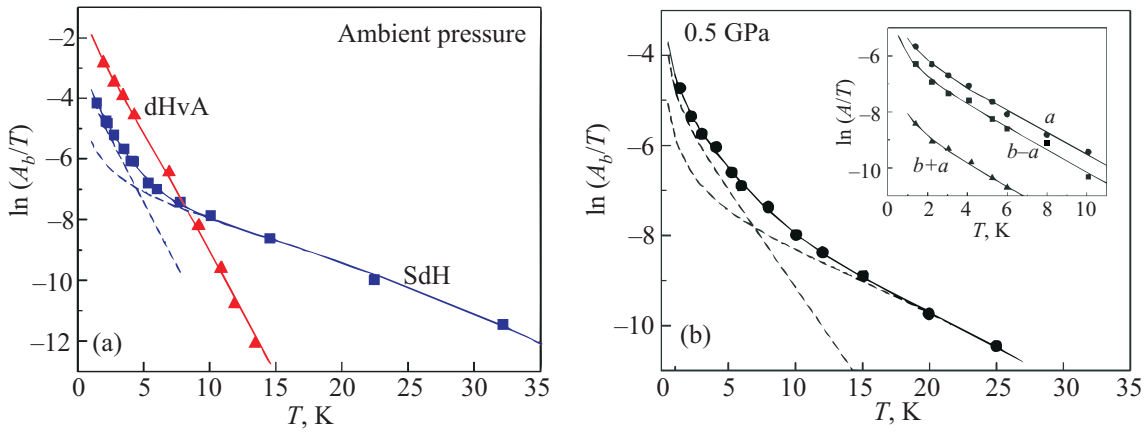

Fig. 4. Temperature dependence of the b oscillations amplitude at (a) 30 and 34.3 T (i.e., 30 T/cos (29°)), respectively, for SdH and dHvA data collected at ambient pressure and (b) 37 T for SdH data collected at 0.5 GPa. Solid squares and solid circles are SdH data collected with the magnetic field perpendicular to the conducting plane. Solid triangles are dHvA data for $\theta = 29°$. Solid lines are the best fits of the LK model assuming either only one closed orbit contributes to the amplitude (dHvA data) or the coexistence of a closed orbit and a quantum interferometer with a zero-effective mass and a temperature-dependent scattering rate (SdH data). Each of these two contributions are displayed as dashed lines. The inset displays data at 0.5 GPa for a, $b - a$ and $b + a$ oscillations at 27, 24 and 30 T, respectively. Solid lines in the inset are the best fits of the LK model assuming only one SdH orbit contributes to the data.

0.5 GPa, respectively. On the basis of the FS reported in Fig. 1(c), and taking into account the opposite sign of the a and b orbits, the $b + a$ component cannot correspond to a MB orbit [14]. In addition, its effective mass (m^*_{b+a} = 0.65 ± 0.10 at 0.5 GPa) is lower than both m^*_a, m^*_{b-a} and, as reported later on, m^*_b. As discussed in Ref. 5, this component which is not observed at ambient pressure has not a semiclassical origin and can be attributed to, e.g., the frequency combinations phenomenon typical of multiband systems [16].

Field dependence of the temperature-independent part of the oscillations amplitude (A/R_T) yields Dingle temperature through Eq. (4), provided contribution of MB can be neglected ($R_{MB} \simeq 1$, see Eq. (5)). Leaving aside the b oscillations for the moment, Eq. (4) holds for a and $b - a$ oscillations. As example, data for SdH $b - a$ oscillations at 0.5 GPa can be considered in Fig. 5 where solid straight lines are the best fits of Eq. (4). Dingle temperatures are $T_D(a) =$ (1.5 ± 1.0) K, $T_D(b-a) =$ (5 ± 1) K at ambient pressure and $T_D(a) =$ (4 ± 1) K, $T_D(b-a) =$ (7 ± 1) K at 0.5 GPa. As already observed in few other ET salts [17], effective masses decrease and Dingle temperatures increase under pressure.

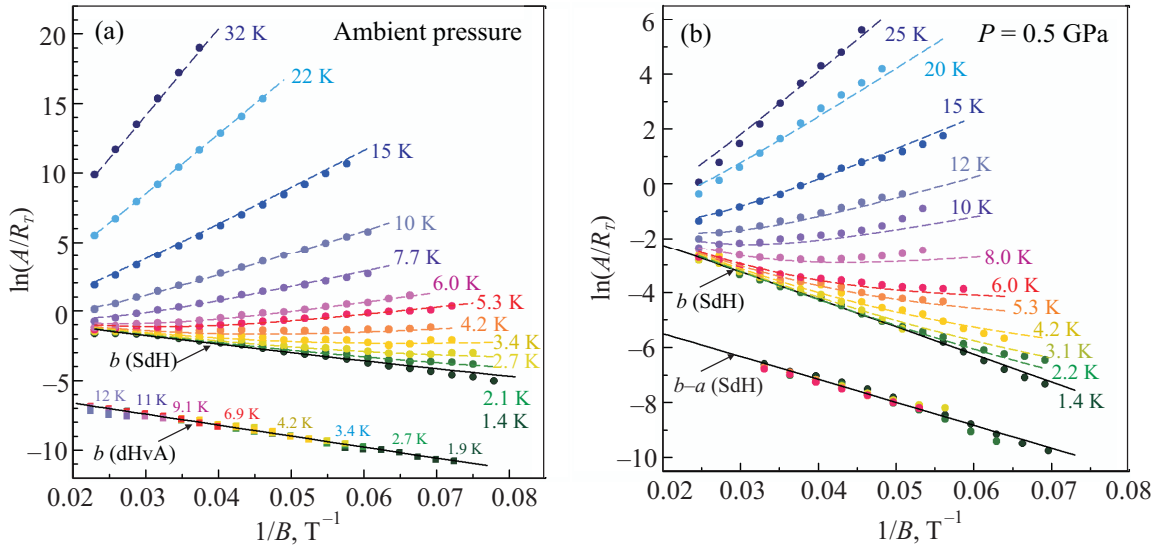

Fig. 5. Dingle plots of (a) SdH and dHvA b oscillations at ambient pressure and (b) b and $b - a$ SdH oscillations at 0.5 GPa (solid symbols). Data for $b - a$ are shifted down for clarity. Solid straight lines are the best fits of Eq. (4) to the data. Dashed lines are calculated assuming that both a SdH orbit and a quantum interferometer contributes to the b oscillation amplitude (see Eq. (10)).

Turn on now to the b oscillations that are observed up to high temperatures in SdH data. Even though dHvA data of Fig. 4 are in agreement with the LK model, a kink is observed in the mass plots of SdH oscillations, at about 8 and 10 K at ambient pressure and 0.5 GPa, respectively, indicating that two phenomena enter the b SdH oscillations amplitude. This is also evidenced in Fig. 4 where, contrary to dHvA data, strong deviations from Eq. (4) are observed for the data relevant to the b SdH oscillations. Although these deviations are larger and larger as the temperature increases, they are detectable at very low temperature (already at 2.7 K at ambient pressure) which suggests that the two phenomena coexist in all the explored temperature range, although with a temperature-dependent weight. The low-temperature part, for which a significant temperature dependence is observed in Fig. 4, can be mainly attributed to SdH effect linked to closed orbit quantization. In contrast, two extreme cases can be considered for the phenomenon responsible for the high-temperature part. Either (i) the damping in this temperature range is also related to a SdH phenomenon, although linked to a closed orbit with an effective mass smaller than in the low-temperature range or (ii) we deal with a symmetric quantum interferometer with a zero-effective mass. This latter hypothesis is considered on the basis of the absence of any kink in the mass plot relevant to dHvA data of Fig. 4(a). Indeed, since magnetization is a thermodynamic parameter, it is only sensitive to the density of states and blind to quantum interference (QI), contrary to resistivity. In the former case (i), neglecting any contribution of MB ($R_{MB} = 1$), the oscillations amplitude is driven by R_T and R_D given by Eqs. (3) and (4). In the latter case (ii), $R_T = 1$ and the damping of the oscillations amplitude as the temperature increases is entirely due to the increase of the inelastic scattering rate τ_i^{-1}. In such a case, $\tau^{-1} = \tau_0^{-1} + \tau_i^{-1}$ where τ_0^{-1} is the temperature-independent elastic part. In the following, it is further assumed that $\tau_i^{-1} \propto T^2$. Besides, in the case of QI, the effective mass entering the Dingle factor (m') is the sum of the partial effective masses of each of the two arms. The Dingle term can therefore be written [18]

$$R_D = \exp[-\frac{\alpha m'}{B}(T_{D0} + \beta T^2)], \tag{7}$$

where β is a constant. Hence the QI amplitude is given by

$$A_{QI} = \exp(p_1 - p_2 T^2), \tag{8}$$

where p_1 and p_2 are given by

$$p_1 = p_{01} - m'\alpha T_{D0}/B, \quad p_2 = \alpha m'\beta/B, \tag{9}$$

where p_{01} is a prefactor. It must be underlined here that Eq. (8) should include a MB factor. However, since nothing is known about the interferometer topology, its field dependence is not known.

Both scenarios (i) and (ii) yield undiscernible mass plots. In other words, solid lines in Fig. 4 can be obtained within the two hypothesis as well, although with different parameters, which prevents deriving any conclusion at this step. Assuming first that the high-temperature part of the oscillatory data is due to SdH effect linked to a closed orbit, the effective mass deduced from mass plots is $m_b^* = 0.35 \pm 0.03$ and 0.31 ± 0.06 at ambient pressure and 0.5 GPa, respectively. Dingle temperatures derived within this hypothesis are unrealistically large ($T_D =$ 7 and 27 K at ambient pressure and 0.5 GPa, respectively) in view of the values observed for a and $b - a$ oscillations, which rules out SdH effect in this temperature range. Considering QI phenomenon instead, the measured oscillations amplitude can be regarded as the sum of the contributions linked to SdH effect dominant at low temperature and QI dominant at high temperature ($A = A_{SdH} + A_{QI}$) provided the two phase factors (γ parameter in Eq. (1)) are the same, which is in agreement with the data (see Fig. 2 and Ref. 18). At a given magnetic field, the temperature dependence of the oscillation amplitude can be written (see Eqs. (3), (4) and (8))

$$A = \exp(p_1 - p_2 T^2) + \frac{T\exp(p_3)}{\sinh(p_4 T)}. \tag{10}$$

According to Eqs. (3) and (4), p_3 and p_4 are given by

$$p_3 = p_{03} - \ln(B) - \alpha m^* T_D / B, \tag{11}$$

$$p_4 = \alpha m^* / B, \tag{12}$$

where p_{03} is a constant. Examples are given in main panels of Fig. 4 where solid lines are the best fits of Eq. (10) to the SdH data at ambient pressure and 0.5 GPa.

Field dependence of the parameters p_1 to p_4 is reported in Fig. 6. First, the field dependence of p_2 is in good agreement with the assumed T^2 dependence of τ_i^{-1} at ambient pressure while, despite large error bars, only a very rough agreement is obtained at 0.5 GPa. This behavior might indicate a departure of the temperature dependence of τ_i^{-1} from the supposed T^2 law under pressure. The field dependence of p_1 and p_3 is in agreement with Eqs. (9) and (11), respectively, within the error bars, which would suggest that Bragg reflections have only a minor contribution to R_{MB} in the applied pressure range studied (see Eq. (5)). Effective mass values deduced from p_4 (see Eq. (12)), which is field-independent within the error bars in the range explored as expected, are $m_b^* = 1.7 \pm 0.2$ and 1.1 ± 0.2 at ambient pressure and 0.5 GPa, respectively. The former value is in agreement with data at ambient pressure deduced from dHvA oscillations ($m_b^* = 1.5 \pm 0.1$) and angle dependence of the SdH oscillations amplitude reported in Fig. 7 (see Eq. (6)): $\mu = 1.6 \pm 0.1$. Regarding these latter data collected at a temperature of 2 K, it can be

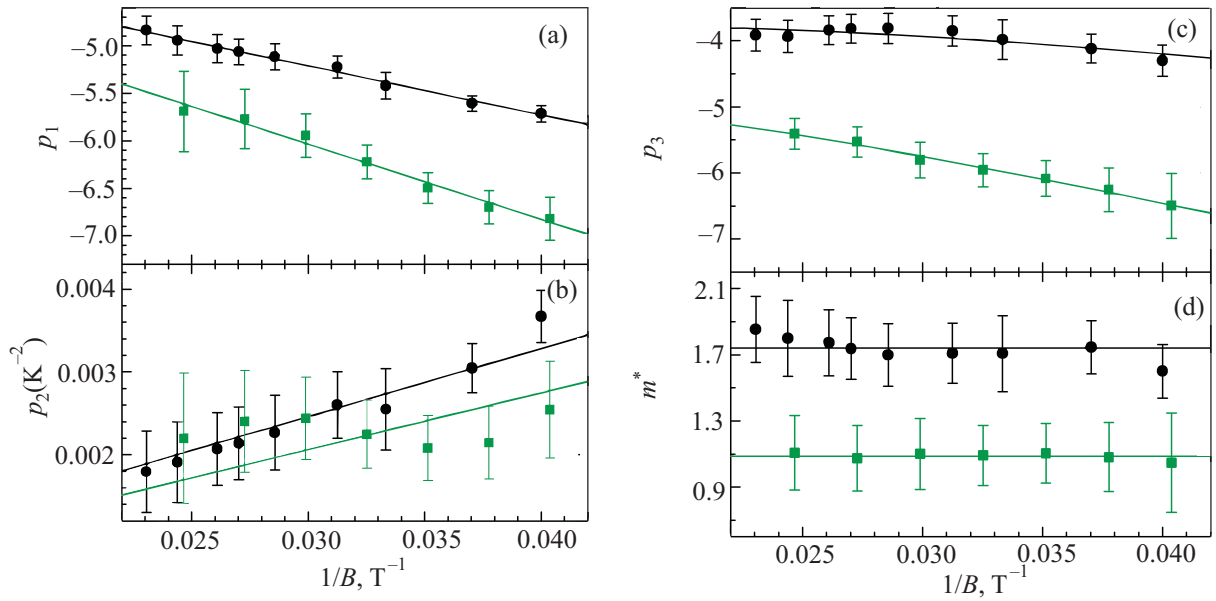

Fig. 6. Field dependence of the parameters (a) p_1, (b) p_2, (c) p_3 and (d) m^* which is proportional to p_4 (see Eq. (12)) relevant to the b oscillations at ambient pressure (solid circles) and 0.5 GPa (solid squares) deduced from the best fits of Eq. (10) to the SdH data of Fig. 3. Solid lines in (a) and (b) are the best fits of Eq. (9). Solid lines in (c) are the best fit of Eq. (11). Horizontal lines in (d) indicate the mean value of the effective mass deduced from p_4.

noticed that, although the two phenomena contributes to the b oscillations amplitude at low temperature, the contribution of closed orbit quantization to the b oscillations amplitude is by a factor about 4 times larger than that of QI at ambient pressure which allow to neglect QI contribution in the data analysis of Fig. 7. Dingle temperatures deduced from p_3 are $T_D = (4 \pm 1)$ K and (6 ± 1) K at ambient pressure and 0.5 GPa, respectively, which is in good agreement with the above reported data for the $b - a$ oscillations. Finally, dashed lines in Fig. 5 are the best fits of Eq. (10) with the above reported parameters: a very good agreement is observed.

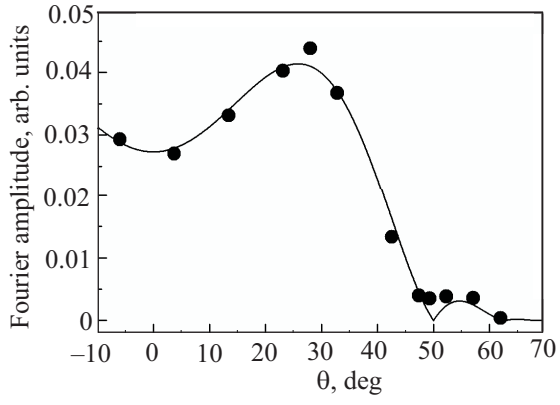

Fig. 7. Angle dependence of the b SdH oscillation amplitude at 2 K. Solid lines are the best fit of Eqs. (3)–(6).

4. Summary and conclusion

Magnetoresistance oscillations spectra of β″-$(ET)_4(H_3O)[Fe(C_2O_4)_3]\cdot C_6H_4Cl_2$ have been studied at ambient pressure and under applied pressure of 0.5 GPa up to 55 T. As it is the case at ambient pressure, several Fourier components are observed, which are linear combinations of two frequencies F_a and F_b. This feature is in line with the textbook case of a Fermi surface composed of three compensated orbits a, $b - a$ and b. However, at variance with de Haas–van Alphen data deduced from magnetic torque measurements, a significant weakening of the thermal damping is observed for the magnetoresistance oscillations relevant to the b Fourier component above temperatures of few Kelvin. As a result, magnetoresistance oscillations can be observed at temperatures as high as 32 K at ambient pressure. Keeping in mind that, as a thermodynamic quantity, oscillatory magnetization is only sensitive to the density of states, this feature can be interpreted on the basis of an additional symmetric quantum interference path with the same area as the b closed orbit and coexisting with it in all the studied temperature range. The question raised by this statement, which remains to be elucidated, deals with the actual Fermi surface topology of the studied compound in magnetic field.

This work has been supported by EuroMagNET II under the EU contract number 228043 and DGES-Spain (Projects FIS2009-12721-C04-03 and CSD2007-00041).

1. E. Coronado and P. Day, *Chem. Rev*. **104**, 5419 (2004).
2. R. Rousseau, M. Gener, and E. Canadell, *Adv. Func. Mater*. **14**, 201 (2004).
3. T.G. Prokhorova, S.S. Khasanov, L.V. Zorina, L.I. Buravov, V.A. Tkacheva, A.A. Baskakov, R.B. Morgunov, M. Gener, E. Canadell, R.P. Shibaeva, and E.B. Yagubskii, *Adv. Funct. Mater*. **13**, 403 (2003).
4. A.D. Dubrovskii, N.G. Spitsina, L.I. Buravov, G.V. Shilov, O.A. Dyachenko, E.B. Yagubskii, V.N. Laukhin, and E. Canadell, *J. Mater. Chem*. **15**, 1248 (2005).
5. A. Audouard, V.N. Laukhin, L. Brossard, T.G. Prokhorova, E.B. Yagubskii, and E. Canadell, *Phys. Rev*. **B69**, 144523 (2004).
6. A. Bangura, A. Coldea, A. Ardavan, J. Singleton, A. Akutsu-Sato, H. Akutsu, and P. Day, *J. Phys. IV* (*France*) **114**, 285 (2004).
7. A. Coldea, A. Bangura, J. Singleton, A. Ardavan, A. Akutsu-Sato, H. Akutsu, S.S. Turner, and P. Day, *Phys. Rev*. **B69**, 085112 (2004).
8. A. Bangura, A. Coldea, J. Singleton, A. Ardavan, A. Akutsu-Sato, H. Akutsu, S.S. Turner, and P. Day, *Phys. Rev.* **B72**, 14543 (2005).
9. D. Vignolles, V.N. Laukhin, A. Audouard, T.G. Prokhorova, E.B. Yagubskii, and E. Canadell, *Eur. Phys. J.* **B51**, 53 (2006).
10. A. Audouard, V.N. Laukhin, J. Béard, D. Vignolles, M. Nardone, E. Canadell, T.G. Prokhorova, and E.B. Yagubskii, *Phys. Rev*. **B74**, 233104 (2006).
11. M. Nardone, A. Audouard, D. Vignolles, and L. Brossard, *Cryogenics* **41**, 175 (2001).
12. E. Ohmichi and T. Osada, *Rev. Sci. Inst*. **73**, 3022 (2002).
13. See, e.g., J. Caulfield, W. Lubczynski, F.L. Pratt, J. Singleton, D.Y.K. Ko, W. Hayes, M. Kurmoo, and P. Day, *J. Phys.: Condens. Matter* **6**, 2911 (1994).
14. L.M. Falicov and H. Stachowiak, *Phys. Rev*. **147**, 505 (1966).
15. D. Shoenberg, *Magnetic Oscillations in Metals*, Cambridge University Press, Cambridge (1984).
16. A.S. Alexandrov and A.M. Bratkovsky, *Phys. Rev. Lett*. **76**, 1308 (1996); *Phys. Lett*. **A234**, 53 (1997), *Phys. Rev*. **B63**, 033105 (2001); P.S. Sandhu, J.H. Kim, and J.S. Brooks, *Phys. Rev*. **B56**, 11566 (1997); J.Y. Fortin and T. Ziman, *Phys. Rev. Lett*. **80**, 3117 (1998); V.M. Gvozdikov, Y.V. Pershin, E. Steep, A.G.M. Jansen, and P. Wyder, *Phys. Rev*. **B65**, 165102 (2002); T. Champel, *ibid*. **65**, 153403 (2002); K. Kishigi and Y. Hasegawa, *ibid*. **65**, 205405 (2002); J.Y. Fortin, E. Perez, and A. Audouard, *ibid*. **71**, 155101 (2005); J.Y. Fortin and A. Audouard, *ibid*. **80**, 214407 (2009).
17. See, e.g., D. Vignolles, A. Audouard, R.B. Lyubovskii, M. Nardone, E. Canadell, and R.N. Lyubovskaya, *Eur. Phys. J*. **B66**, 489 (2008) and references herein.
18. D. Vignolles, A. Audouard, V.N. Laukhin, E. Canadell, T.G. Prokhorova, and E.B. Yagubskii, *Eur. Phys. J*. **B71**, 203 (2009).